

COMPUTATIONAL FLUID DYNAMICS USED IN THE DESIGN OF WATERBLAST TOOLING

J. Schneider
StoneAge, Inc.
Durango, Colorado, U.S.A.

ABSTRACT

Advancements in computer technology in the last decade have made analysis and simulation programs more capable and commercially available. SolidWorks Flow Simulation is a computational fluid dynamics software package designed to analyze fluid flow. Modeling allows for parts and systems to be optimized virtually and reduces prototype manufacturing; this saves time and money during product development.

Analysis using SolidWorks Flow Simulation was performed on models of physical test setups. The program's input parameters and output variables were refined and selected to best reproduce the physical performance testing of waterjets. Flow rates ranging between 40L/min (10.5gpm) and 160L/min (42gpm) at a pressure of 69MPa (10,000psi) were tested. The simulation results were then compared with empirical data to determine if computational fluid dynamics performed by SolidWorks Flow Simulation could be effectively utilized in the design of waterblast tooling.

1. INTRODUCTION

In the waterblast industry it is commonly necessary for the design of a part or system to be optimized for fluid flow characteristics and manufacturability using computer analysis. The best options for machined features, feeder tube selections or even entire flow path designs can be assessed earlier in the design, or in a more comprehensive way.

SolidWorks Flow Simulation was the software package used for this paper to analyze how water flows through the 3D models created in the base CAD program, SolidWorks. Several simulations were set up and run to create and test a validation model for the results described in the paper *The Effect of Upstream Feeder Tube Diameter and Length on Waterjet Performance in Cleaning Applications* by Doug Wright, published in the 2015 WJTA proceedings.

2. SIMULATION CONFIGURATIONS AND SETUP

The analysis performed in this paper was comprised of different combinations of three separate tube diameters, in three lengths, with three different orifice sizes. The tube inside diameters were 7.9mm (.312"), 20.7mm (.815") and 27.9mm (1.10"). The three lengths were 102mm (4"), 305mm (12"), and 914mm (36"). The three orifice diameters were 1.6mm (.063"), 2.3mm (.090") and 3.2mm (.125").

The simulation parameters were held constant across all simulations. The analysis was internal using liquid water at 20°C (68°F) with a .4µm (16µin) surface roughness. The turbulence model used was Intensity and Length with the default parameters set at 2% and 1.05mm (.0413"). A static pressure inlet boundary condition of 69MPa (10,000psi) was used in conjunction with an outlet volume flow boundary condition with respect to each orifice size, set at 40L/min (10.5gpm), 83L/min (22gpm) and 160L/min (42gpm), as shown in Figure 1. The code in program was not written to calculate the mixing of two media, such as a waterjet shooting into air. A water chamber was added after the orifice to allow the mesh to fully resolve the waterjet and to locate the outlet flow boundary condition.

3. MESH AND RESULTS ANALYSIS

3.1 Mesh

The mesh settings and strategy had an overwhelming influence on the results produced. Several mesh refinements were made on the initial models in an effort to produce the most consistent results across all the configurations before the final studies were solved.

Control planes were set up to center the mesh on the axes of the inlet and the feeder tube/ orifice, shown in Figure 1. Centering the mesh reduced the number of cells needed to resolve the features and allowed the mesh to better represent the symmetrical nature of the tubes and orifice. A courser global mesh was used to analyze the inlet, head, and feeder tube, shown in Figure 2. The final

mesh produced a result of 12 cells across a given diameter and was tailored to resolve the bulk of the flow.

Three local meshes were used to resolve the transition into the orifice, the orifice itself and the region immediately following the orifice. Local meshes allow for specific refinement in key areas of interest or concern, usually known by the designer, which may not be resolved as well when left up to the program's general mesh refinement process. A meshing technique was used utilizing solid parts inserted into the flow regime to provide a volume around which the program could specifically refine the mesh. These solids were disabled, or set so they did not change or influence the flow path. The finer local mesh and the mesh solids are shown in Figure 3. The mesh created by these local settings had an elevated level of curvature refinement and produced 24-28 cells across the flow path to better resolve the bulk of the fluid flow and account for the influence of the significantly changing geometry.

Numerical values in a cross section of the flow were calculated by taking the values from each cell and averaging them. When the number of cells across the diameter was increased it produced a result which was less influenced by the zero-slip wall conditions. The actual value produced was directly related to the cell count until convergence was neared by having a sufficient number of mesh cells. An adaptive mesh, which refined the mesh during the calculation in areas with a high gradient was also explored. However, with the results correlating to the number of mesh cells, an adaptive mesh was not used in order to eliminate any additional source of error due to a difference in number of cells between the studies. Each model had between 150,000 and 250,000 mesh cells with approximately 60% being fluid cells and the majority of the remaining cells being partial cells.

3.2 Results Analysis

Two styles of results were produced by the program, numerical and pictorial. Average values taken from the cross section of the fluid at the end of the orifice were used for the numerical results. These results are graphed in Figures 5, 7, 9, 10, and 11. The physical performance test results are graphed in Figures 4, 6, and 8. Images depicting the flow in cross sections parallel to and perpendicular to the orifice axis can be found in Figures 12 through 23.

3.2.1 Physical Performance Test Results

In the paper *The Effect of Upstream Feeder Tube Diameter and Length on Waterjet Performance in Cleaning Applications* by Doug Wright, an improvement in the physical cutting performance of a waterjet was found by increasing either the length of the feeder tube and/or the diameter of the feeder tube in order to achieve more ideal upstream conditions. One set of results shown in Figures 4, 6, and 8, illustrate a percent performance improvement in terms of the ratio of the tube inside diameter divided by the orifice diameter for three separate lengths of tube. Another data trend indicated the optimal tube diameter shifted toward a larger tube inside diameter as the length was increased.

3.2.2 Numerical Results

As part of the setup for a simulation, goals were created. Goals are used as convergence criteria and help tailor the equations being solved for each cell in the mesh to produce the desired output. Surface goals of average volume flow rate and average total pressure were created for the cross section of the flow where the waterjet exits the orifice. In Figures 5, 7, and 9, the ratio of the tube inside diameter divided by the orifice diameter for three separate length of tube were plotted against the total pressure at the orifice.

Total Pressure at the orifice was found to be the output parameter which most closely followed the physical test results for each setup; however, the trend of the curves did not fully reproduce the physical performance curves. Total pressure is the static pressure plus the dynamic pressure. Dynamic pressure is the density of the fluid times one half the velocity squared. In varying the number of mesh cells across the orifice, some studies which had as few as 14 cells showed a better correlation to the physical results. This suggests the zero-slip wall condition and the boundary layer formation have a significant influence on the jet quality, and increasing the number of mesh cells may damp out the realistic magnitude of this influence. In the manufacturing of a nozzle the surface finish in the orifice has a measurable impact on the waterjet performance, which influences the boundary layer formation and supports this correlation.

Other parameters were explored including waterjet velocity and turbulence intensity; these results are graphed in Figures 10 and 11 for the 305mm (12”) length tube. The average velocity of the waterjet as it exited the orifice did not trend with the physical results. With a larger diameter feeder tube, the velocity in the feeder tube is slower because velocity is directly driven by the diameter and flow rate. This might have been what influenced the waterjet and decreased the exit velocity. In the physical tests, the larger tube diameters generally increased the waterjet performance. Further investigation is needed to determine if these results show an inverse effect correlating a lower velocity waterjet as an indicator of jet quality. The average turbulence intensity of the cross section of the flow at the orifice also does not fully represent the physical data. Figure 11 shows the smaller diameter tubes had less turbulence than the larger diameters; however, the larger tubes produced better performing waterjets. In nozzle design and testing, a more cohesive jet has better cutting performance. Assuming the energy of a cohesive waterjet is more focused, it would be expected to have a lower turbulence intensity, which is not represented by this data set.

3.2.3 Image Results

Turbulence intensity provided the strongest visual representation of how the water flowed through the system. These plots overlaid with velocity streamlines in a cross section parallel to the flow are shown in Figures 12 through 17. The water started out smooth and uniform, gained turbulence as it changed direction, and then again smoothed out as it traveled the remaining length of the feeder tube. These plots show that the larger diameter tubes took more length to smooth out the turbulence than the smaller diameter tubes. The large diameters had a less constricting effect at the entry into the feeder tube and allowed a recirculation zone to form. This supports the physical results which indicated a minimum tube length to tube inside diameter ratio must be maintained and is suggestive of the physical data that showed the optimum inside diameter trending larger with increased length.

Figures 18 through 23 show several cross sections perpendicular to the flow, with a turbulence intensity plot overlaid by velocity vectors. These plots show how the water moved in a direction other than axially down the tube. A shift in characteristics happened as the length was increased. A dual recirculation effect could be seen where the water from the cavity in the head entered the feeder tube from each side while it was rotating in opposite directions. Over the length of the longer tubes the dual recirculation dampened out and the flow combined into one rotation direction before it reached the orifice. In the shorter lengths and smaller diameter tubes the flow reached the orifice before it had time to unify. The opposed rotation can be seen in the first cross section on the left side of Figures 18, 19 and 21 for the 7.9mm (.312") inside diameter tube in the 102mm (4") and 305mm (12") long tubes, and also in the 27.9mm (1.1") inside diameter, 102mm (4") tube. In the physical performance graph of Figure 4, the performance reached 60% by the time the rotation was unified. This dynamic influence may be a contributing effect to the optimal tube inside diameter to orifice diameter ratio being 5-7 for a 3.2mm (.125") orifice size, while maintaining a minimum length to tube inside diameter ratio.

3.2.3 Flow Simulation Capabilities

The results obtained in these studies were achieved by attempting several different approaches and using the one which fit best. A further investigation would lead to utilizing more advanced meshing techniques, researching and optimizing the turbulence model parameters, and a more strategic use of goals to leverage their interdependence to produce the desired results. Significant attention would need to be given to setting up every model in a proper, unified method due to the difference in comparative results being 1% to 3% of the input value.

The physical performance of a waterjet is determined by many variables which can be heavily influenced by slight changes. These studies have shown that of the parameters explored, including pressure drop and waterjet velocity, waterjet performance is not dependent on just a single output parameter.

4. CONCLUSION

SolidWorks Flow Simulation provides a variety of unique ways to extract data. Numerical data can be used to calculate pressure drop and velocities, and the imagery can answer questions about geometrical features, help explain effects present in test data and build intuition about the fluid dynamics of a system. Simulation studies looking for physical cutting performance results for waterjet are pushing the limits and require a deep knowledge of the program. While the results produced were not able to reliably predict the physical test results, they did follow the trend and shed light on the fluid dynamics involved in a feeder tube and orifice system. Flow Simulation is a viable tool to aid in the design of waterblast tooling but is not a replacement for physical performance testing at this point in time.

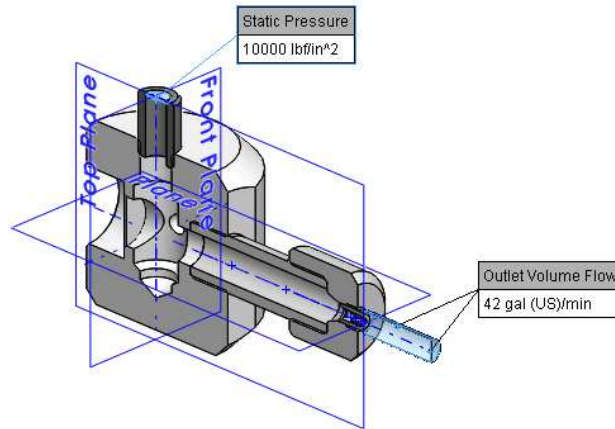


Figure 1: Shown are Mesh Control Planes and the Model Boundary Conditions of 69MPa (10,000psi) and 160L/min (42gpm) for the 20.7mm (.815”) Inside Diameter, 102mm (4”) Long Tube with 3.2mm (.125”) Orifice

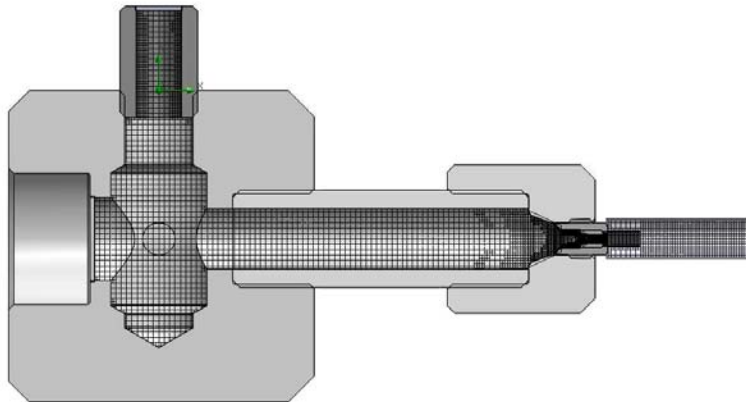


Figure 2: Global Mesh - Showing 20.7mm (.815”) Inside Diameter, 102mm (4”) Long Tube with 3.2mm (.125”) Orifice

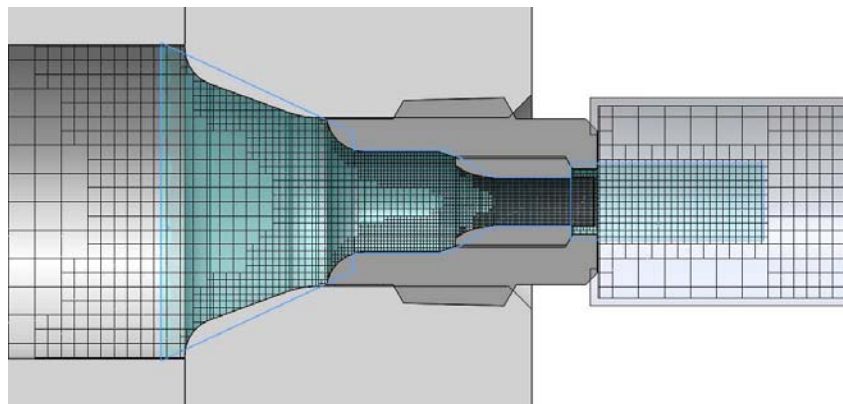


Figure 3: Local Mesh Refinement at the Orifice using Mesh Solids - 20.7mm (.815”) Inside Diameter Tube with 3.2mm (.125”) Orifice

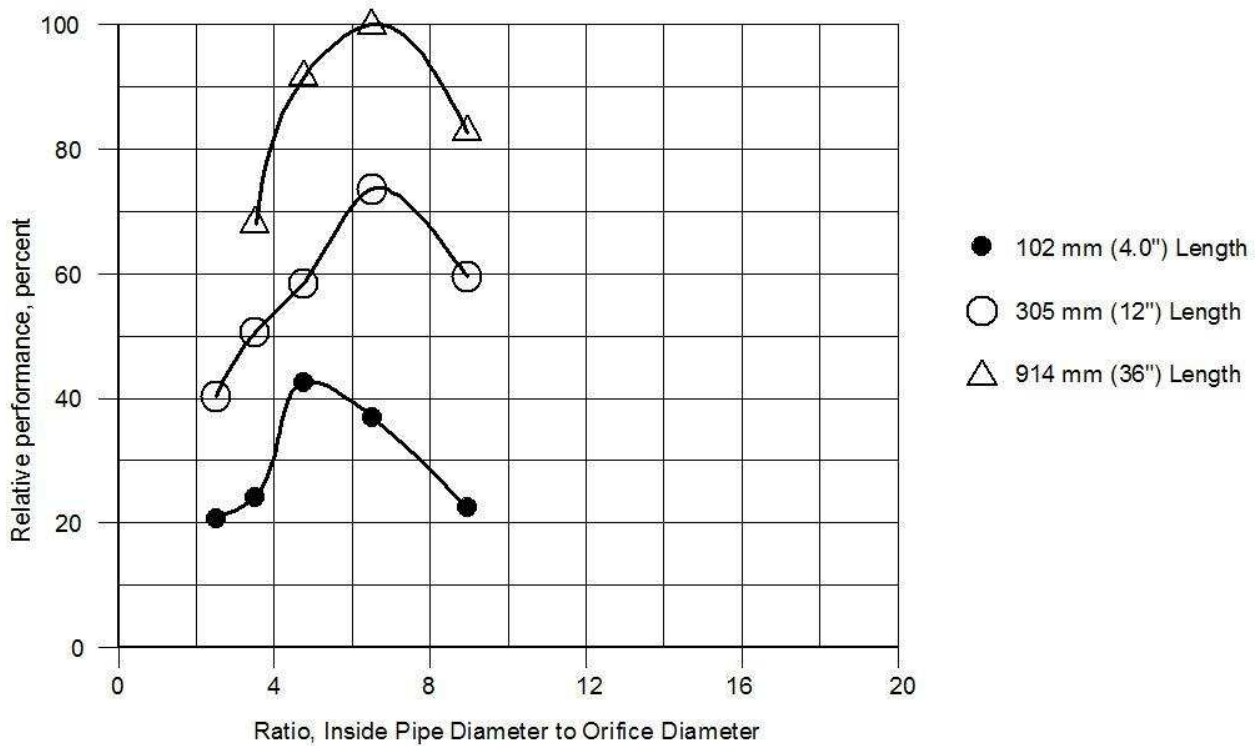


Figure 4: Relative Performance with Increasing Feeder Tube Inside Diameter at 3.2 mm (.125") Orifice Size

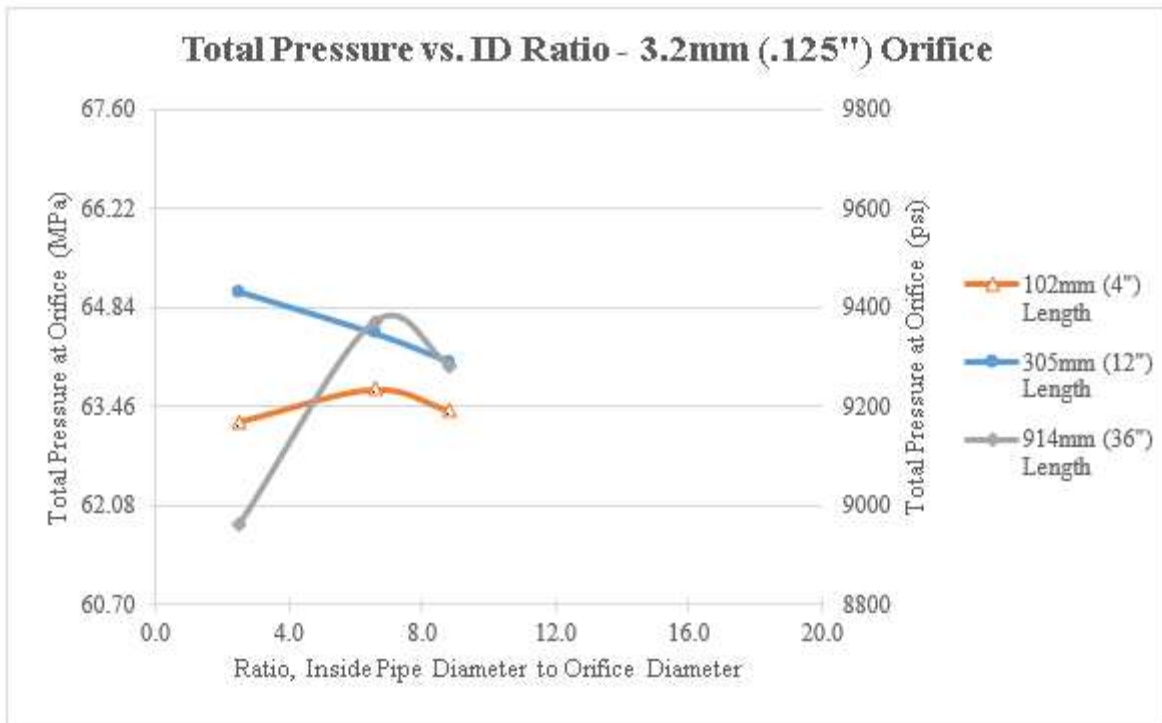


Figure 5: Simulation Results using Total Pressure as an Indicator of Relative Performance for a 3.2mm (.125") Orifice Size

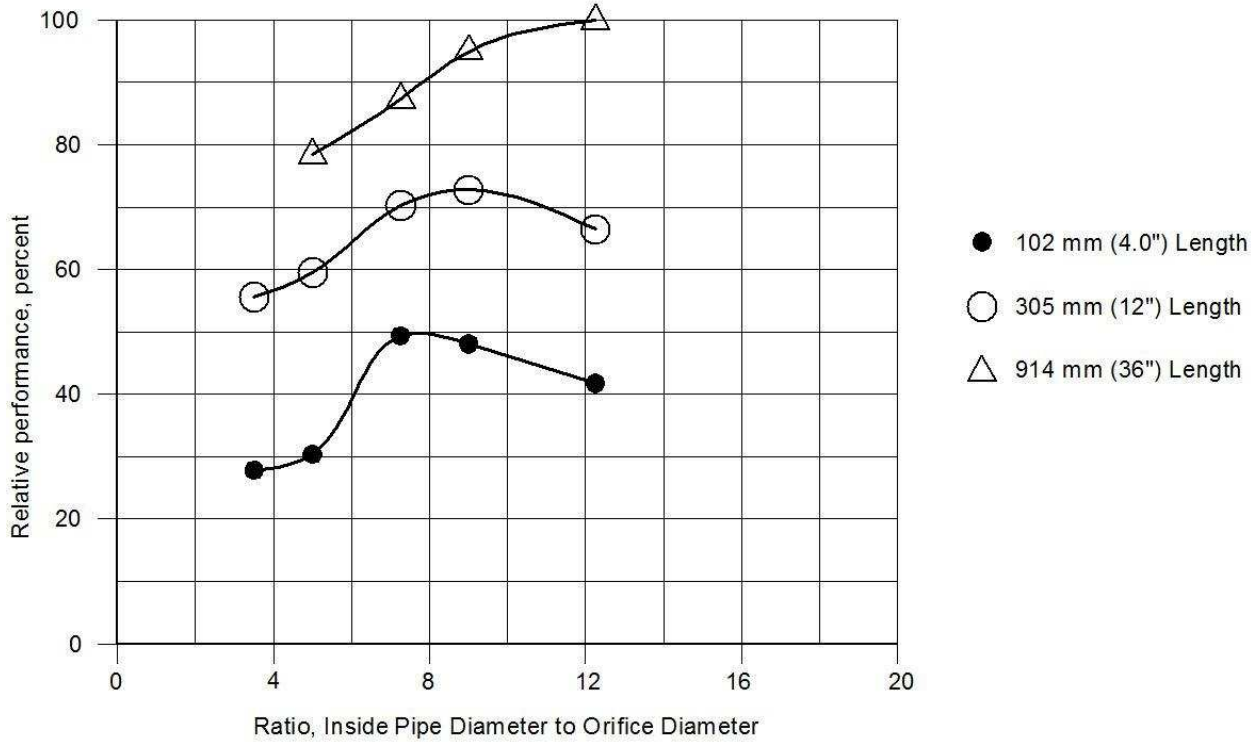


Figure 6: Relative Performance with Increasing Feeder Tube Inside Diameter at 2.3 mm (.090\") Orifice Size

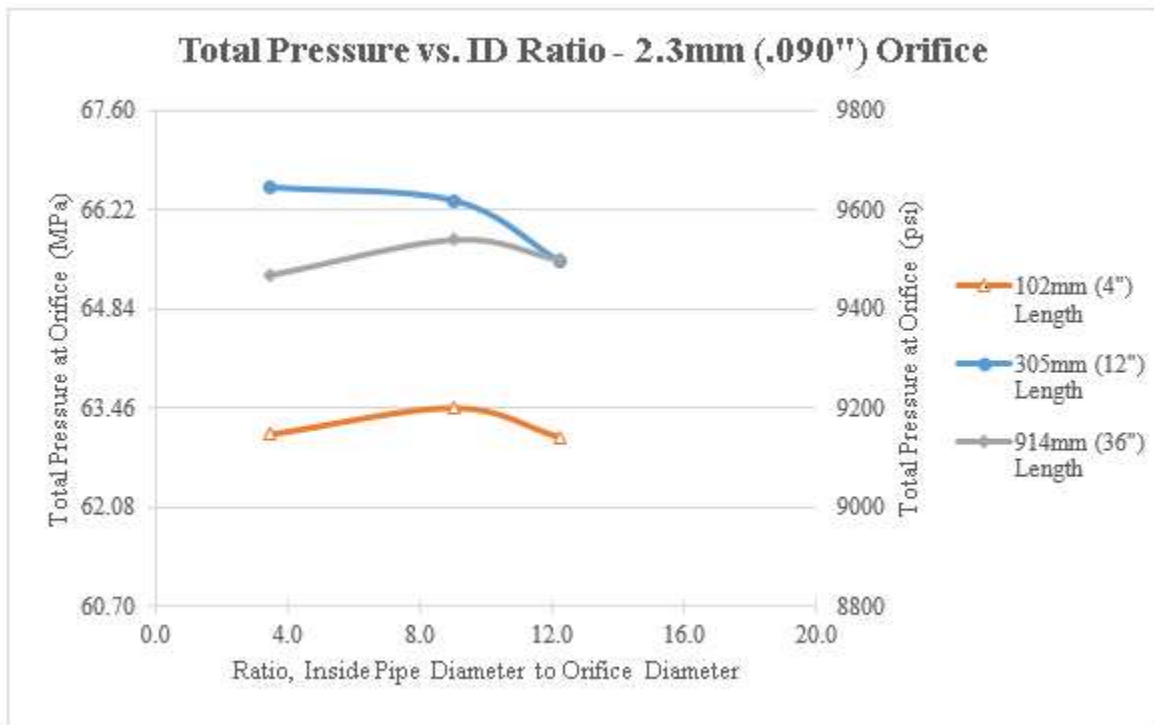


Figure 7: Simulation Results using Total Pressure as an Indicator of Relative Performance for a 2.3mm (.090\") Orifice Size

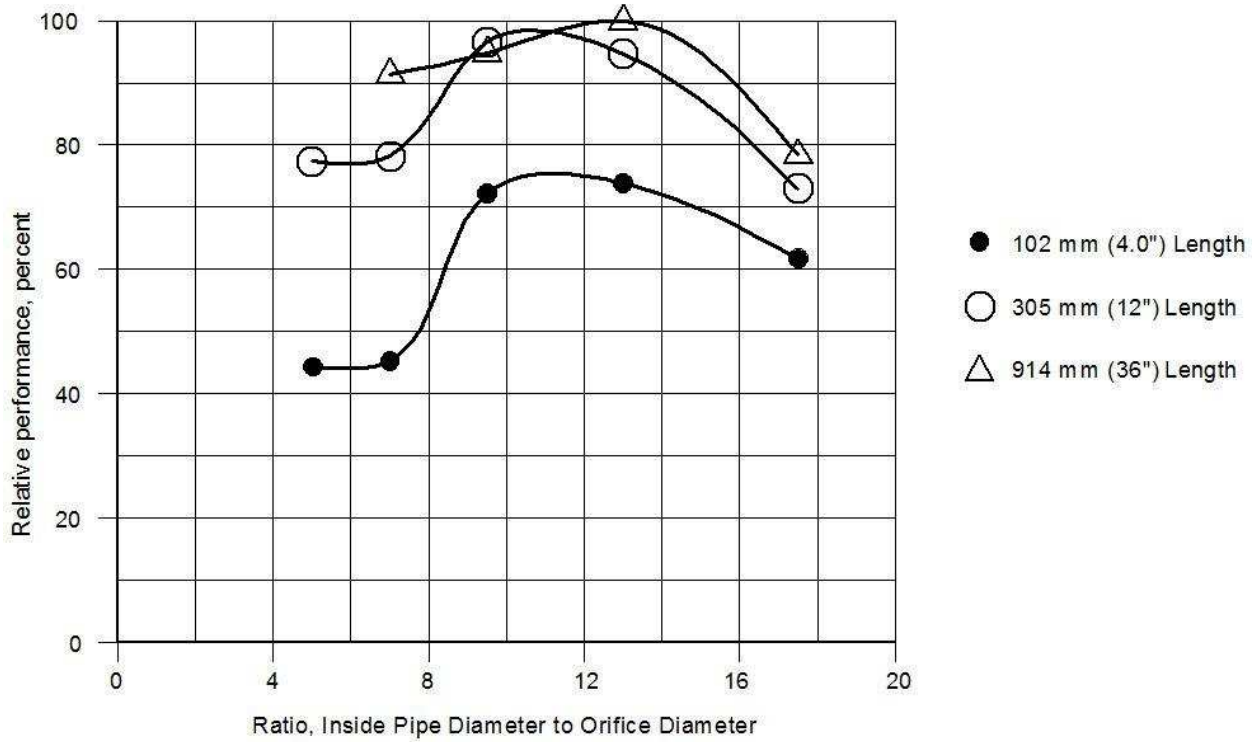


Figure 8: Relative Performance with Increasing Feeder Tube Inside Diameter at 1.6 mm (.063") Orifice Size

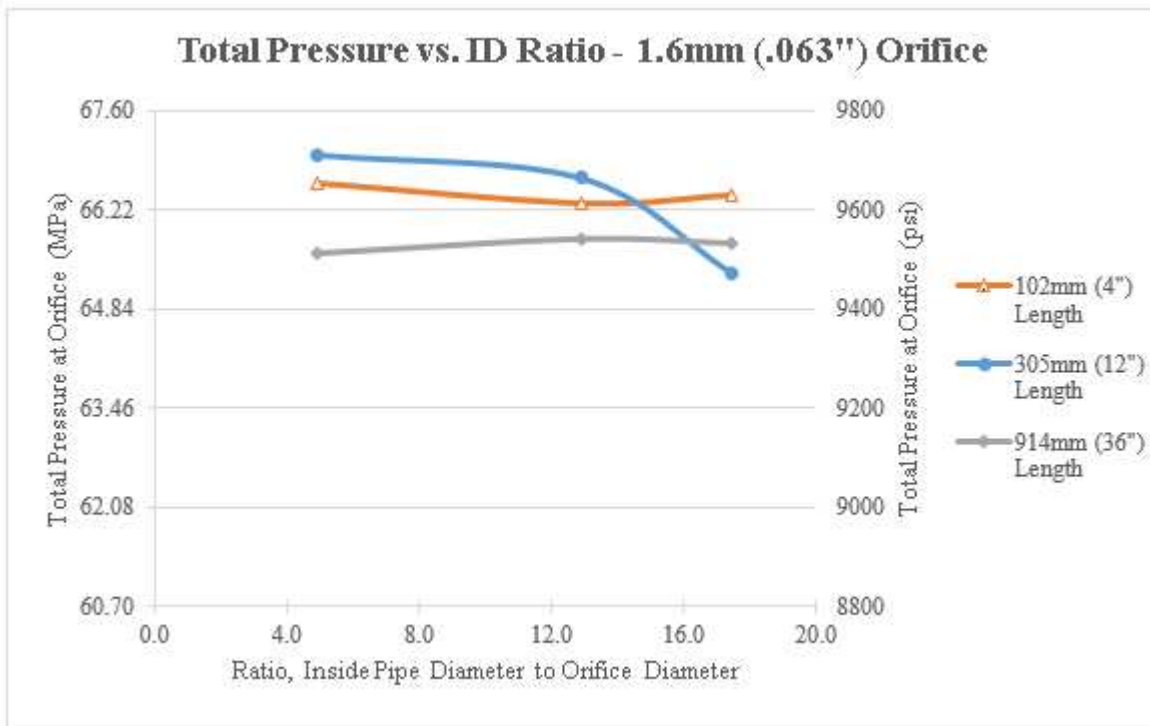


Figure 9: Simulation Results using Total Pressure as an Indicator of Relative Performance for a 1.6mm (.063") Orifice Size

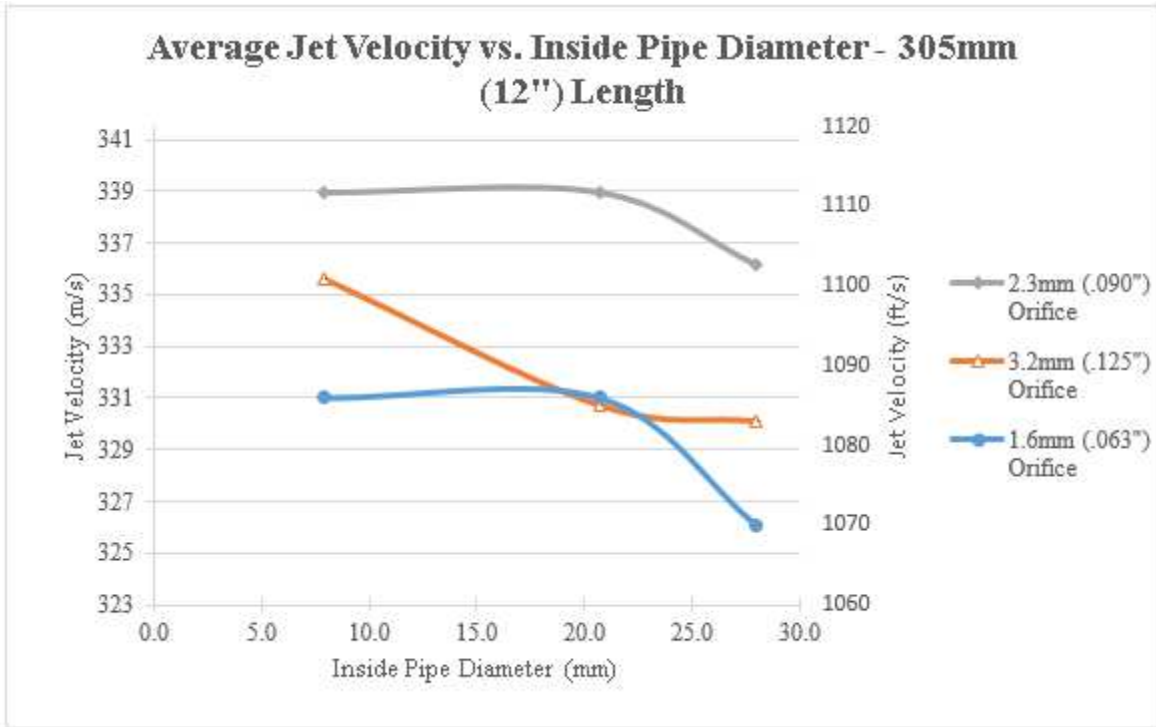


Figure 10: Simulation Results Correlating the Velocity of the waterjet to the Inside Tube Diameter for each Orifice Diameter

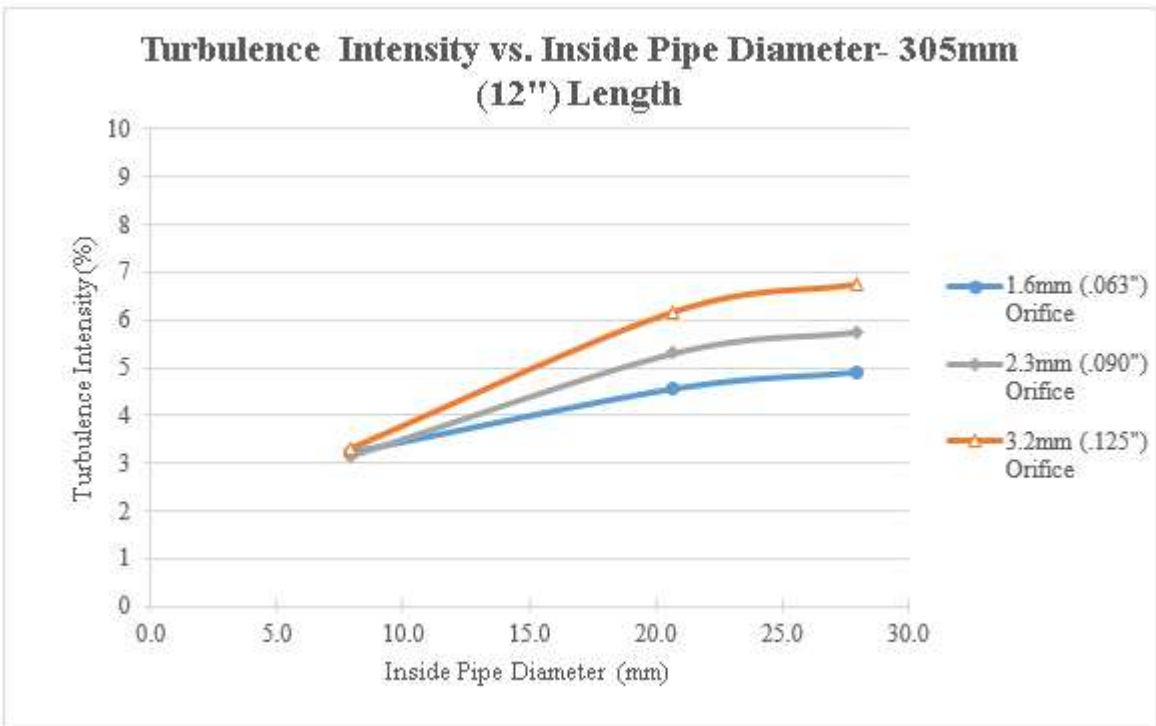


Figure 11: Simulation Results Correlating the Percent Turbulence Intensity of the waterjet to the Inside Tube Diameter for each Orifice Diameter

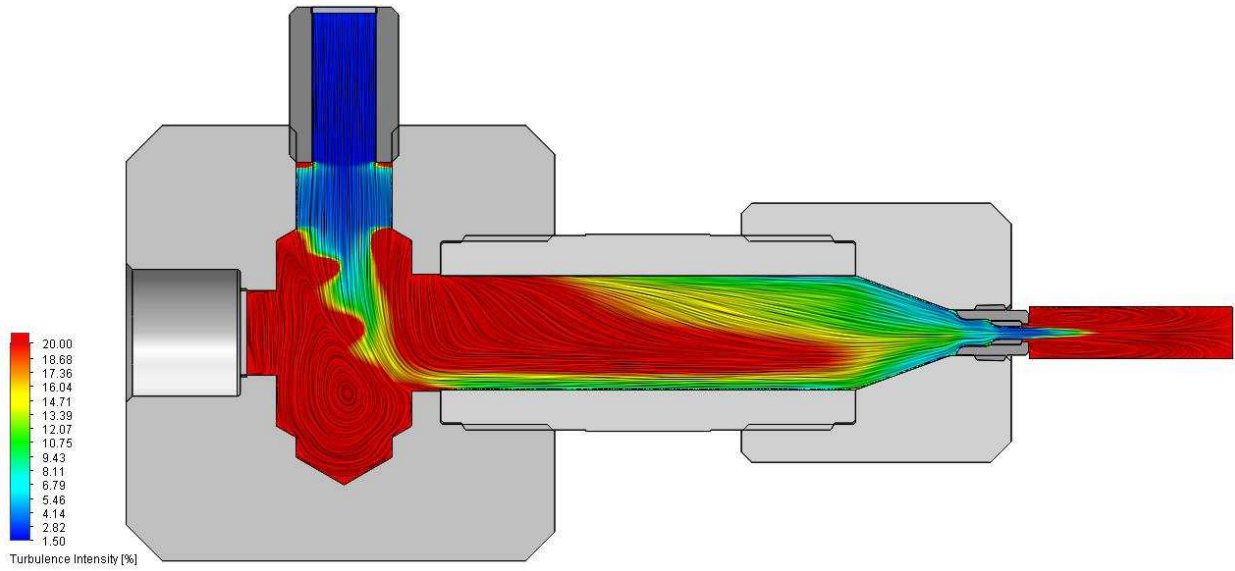


Figure 12: Turbulence Intensity with an Overlay of Velocity Streamlines - Showing 27.9mm (1.1") Inside Diameter, 102mm (4") Long Tube with 3.2mm (.125") Orifice

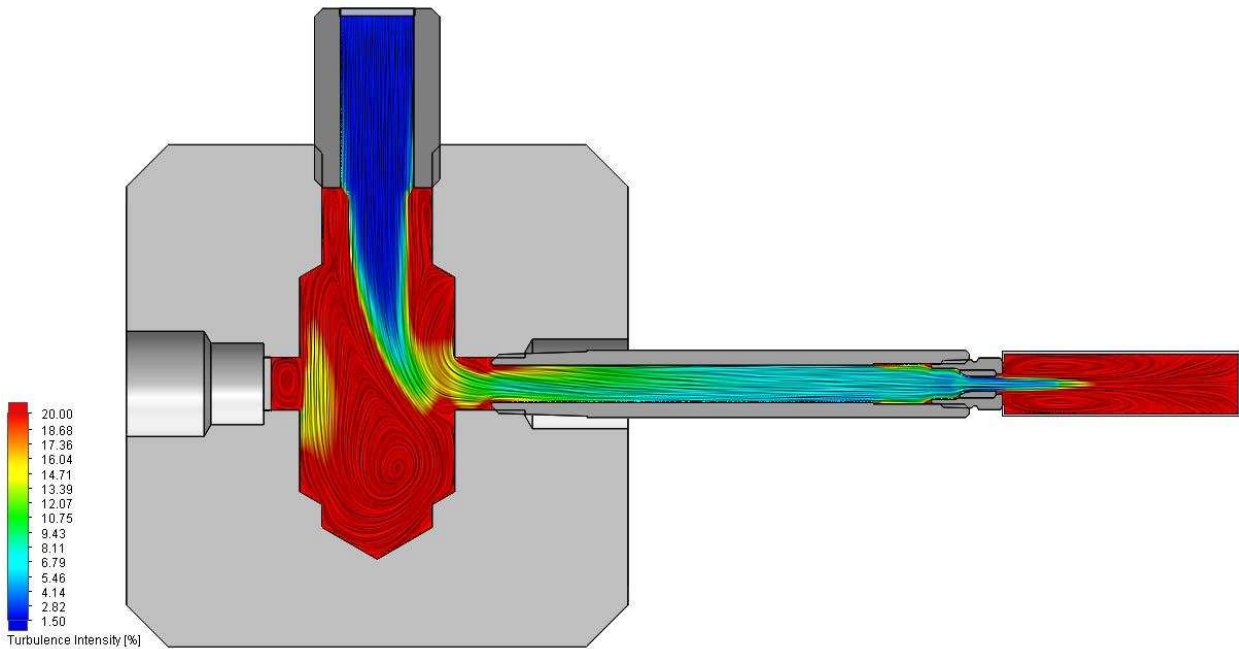


Figure 13: Turbulence Intensity with an Overlay of Velocity Streamlines - Showing 7.9mm (.312") Inside Diameter, 102mm (4") Long Tube with 3.2mm (.125") Orifice

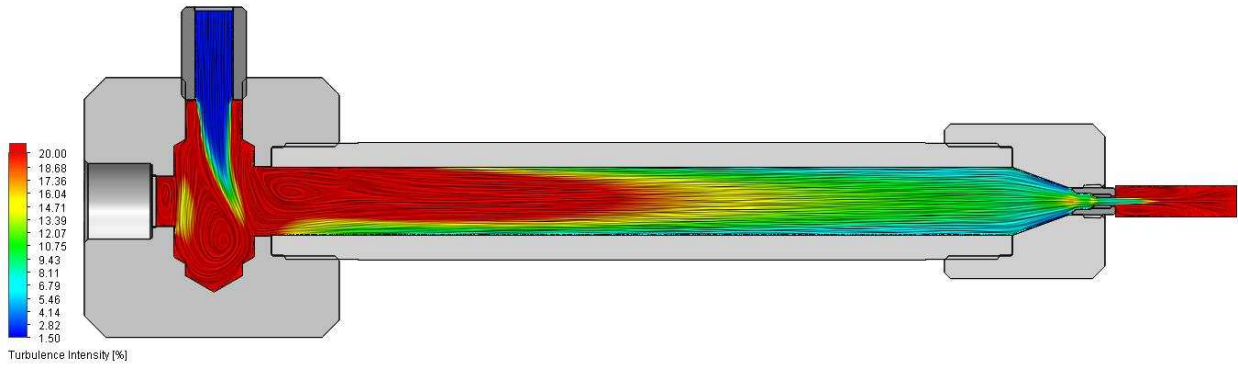


Figure 14: Turbulence Intensity with an Overlay of Velocity Streamlines - Showing 27.9mm (1.1") Inside Diameter, 305mm (12") Long Tube with 3.2mm (.125") Orifice

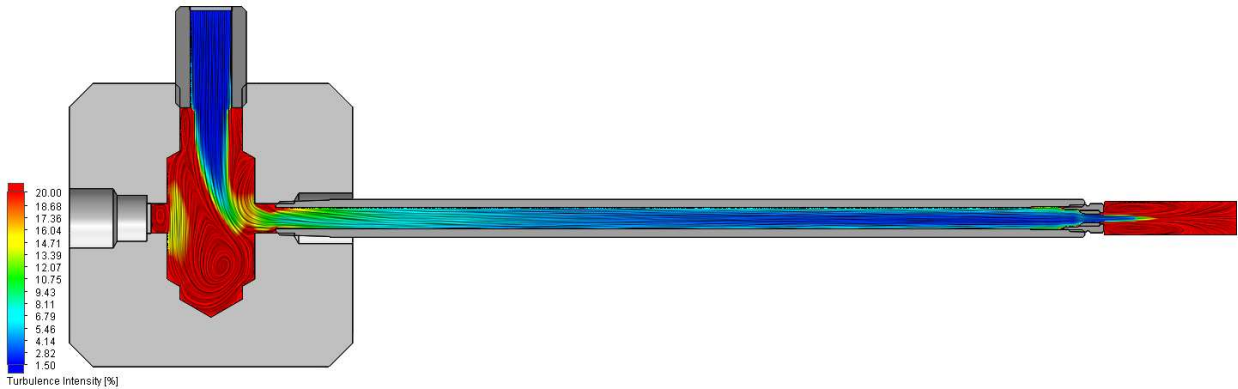


Figure 15: Turbulence Intensity with an Overlay of Velocity Streamlines - Showing 7.9mm (.312") Inside Diameter, 305mm (12") Long Tube with 3.2mm (.125") Orifice



Figure 16: Turbulence Intensity with an Overlay of Velocity Streamlines - Showing 27.9mm (1.1") Inside Diameter, 914mm (36") Long Tube with 3.2mm (.125") Orifice



Figure 17: Turbulence Intensity with an Overlay of Velocity Streamlines - Showing 7.9mm (.312") Inside Diameter, 914mm (36") Long Tube with 3.2mm (.125") Orifice

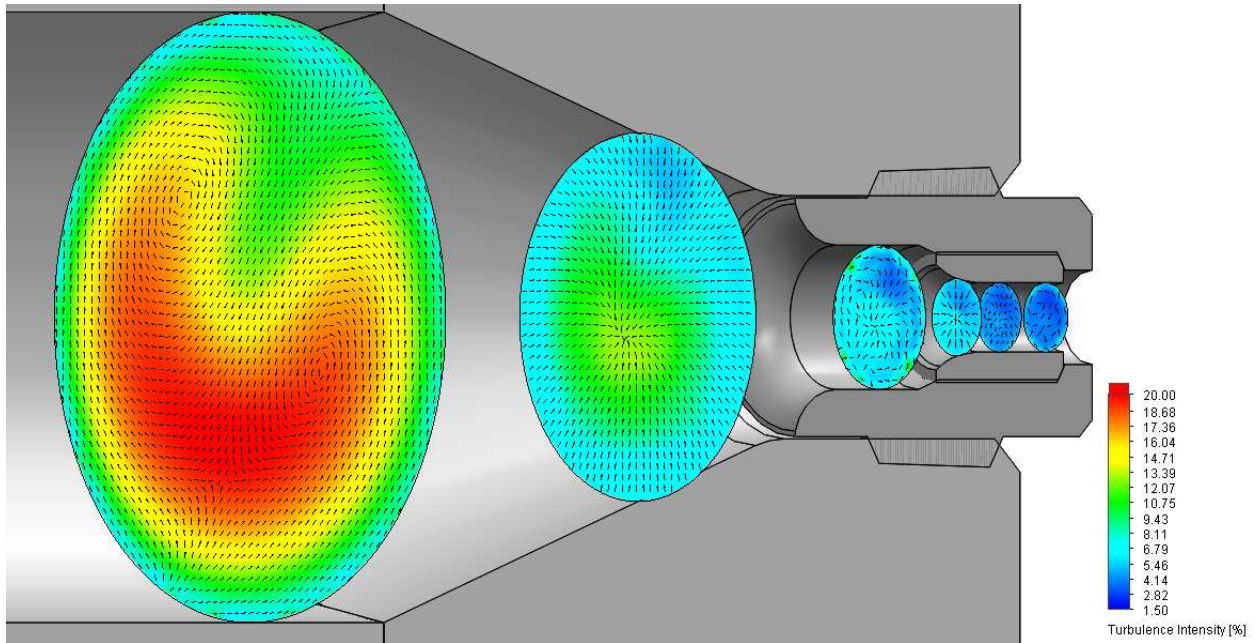


Figure 18: Turbulence Intensity with an Overlay of Velocity Vectors - Showing 27.9mm (1.1") Inside Diameter, 102mm (4") Long Tube with 3.2mm (.125") Orifice

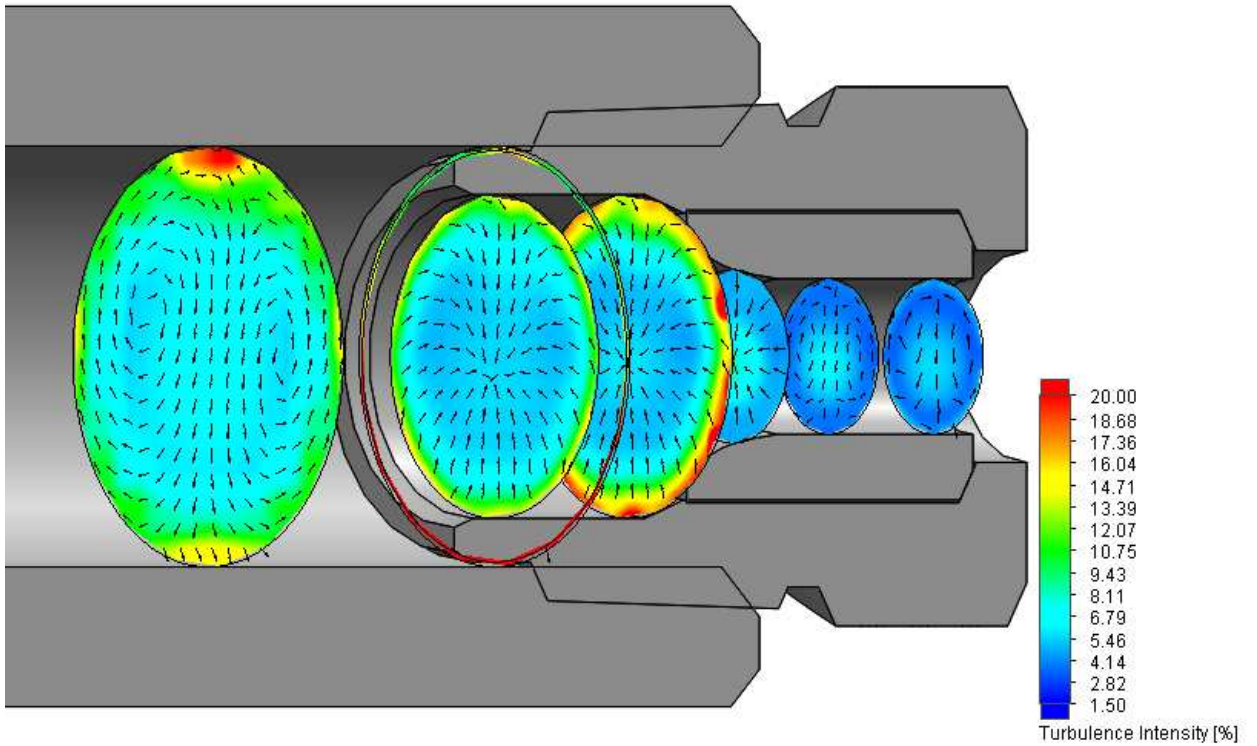


Figure 19: Turbulence Intensity with an Overlay of Velocity Vectors - Showing 7.9mm (.312") Inside Diameter, 102mm (4") Long Tube with 3.2mm (.125") Orifice

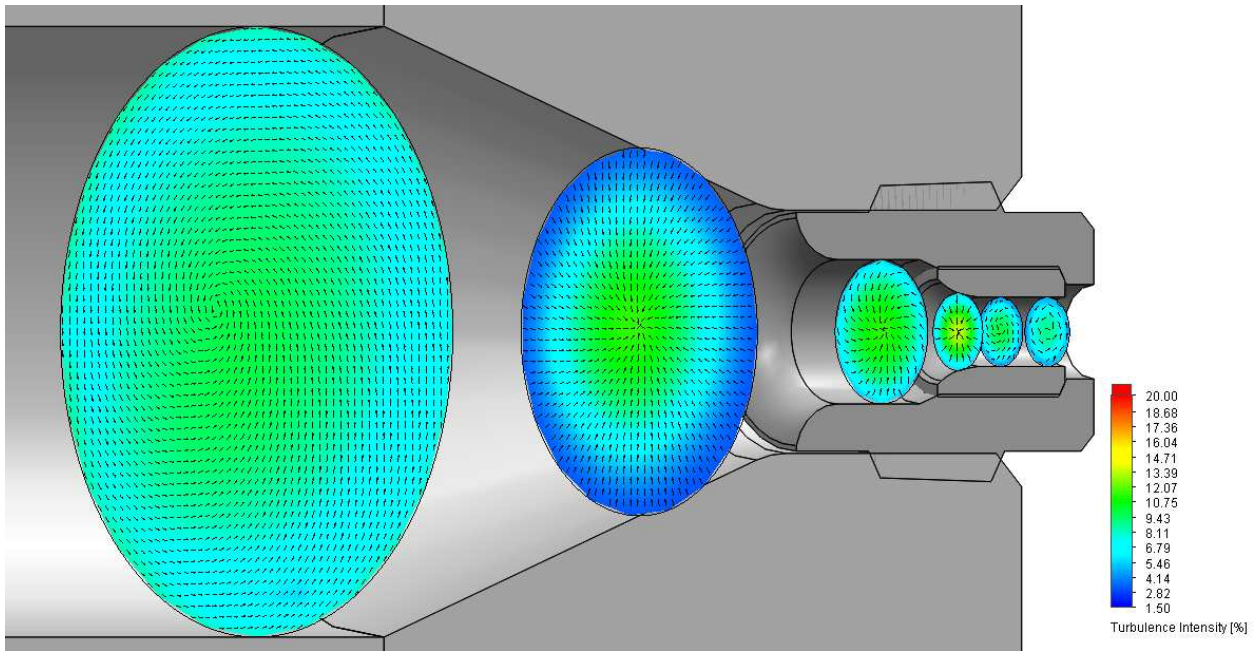


Figure 20: Turbulence Intensity with an Overlay of Velocity Vectors - Showing 27.9mm (1.1") Inside Diameter, 305mm (12") Long Tube with 3.2mm (.125") Orifice

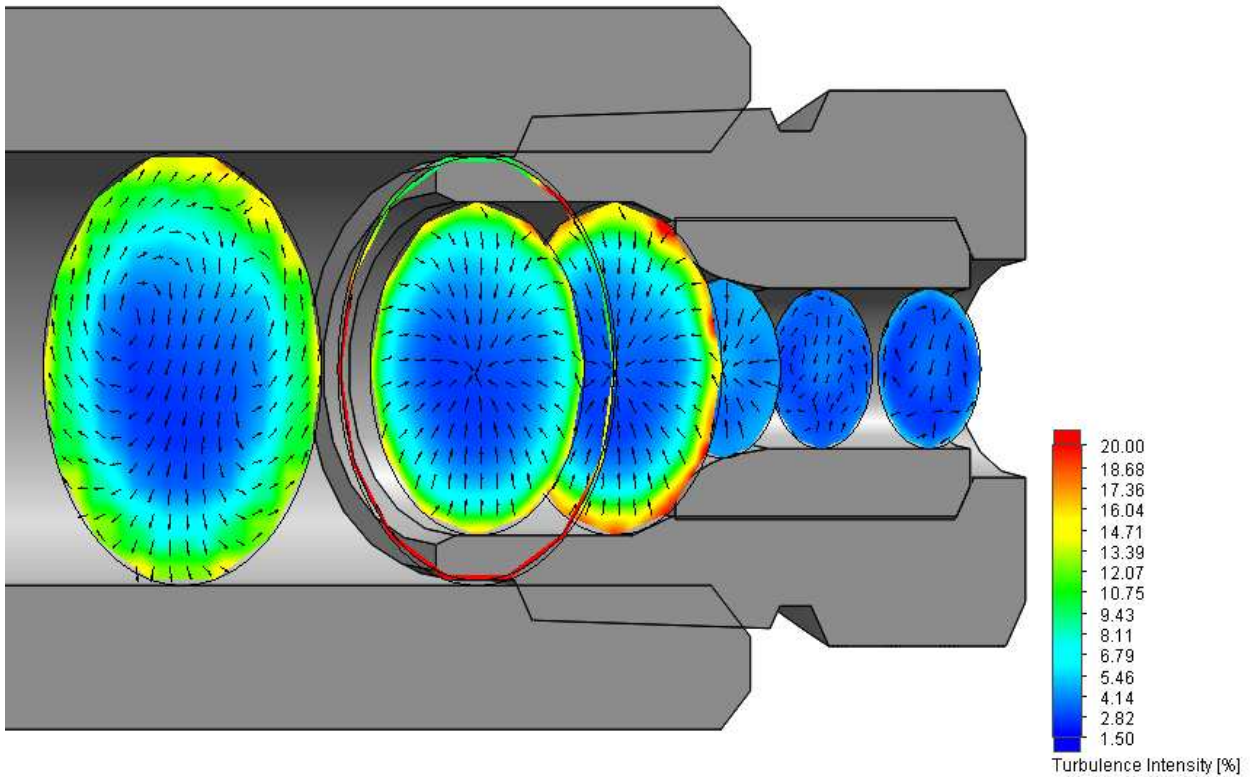


Figure 21: Turbulence Intensity with an Overlay of Velocity Streamlines - Showing 7.9mm (.312") Inside Diameter, 305mm (12") Long Tube with 3.2mm (.125") Orifice

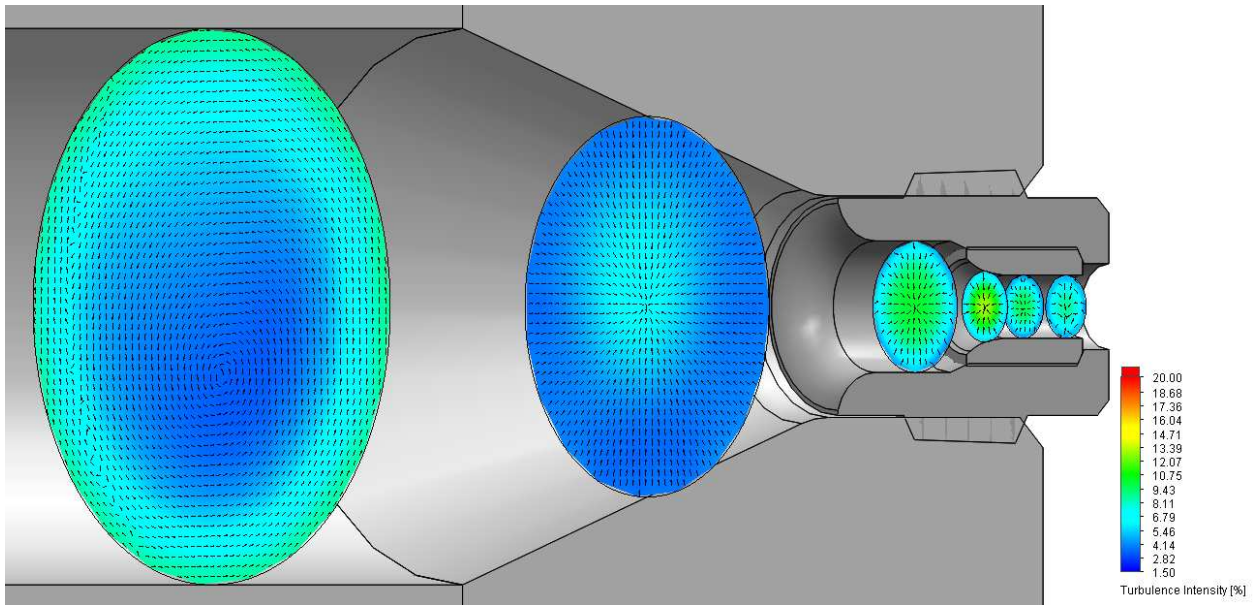


Figure 22: Turbulence Intensity with an Overlay of Velocity Vectors - Showing 27.9mm (1.1") Inside Diameter, 914mm (36") Long Tube with 3.2mm (.125") Orifice

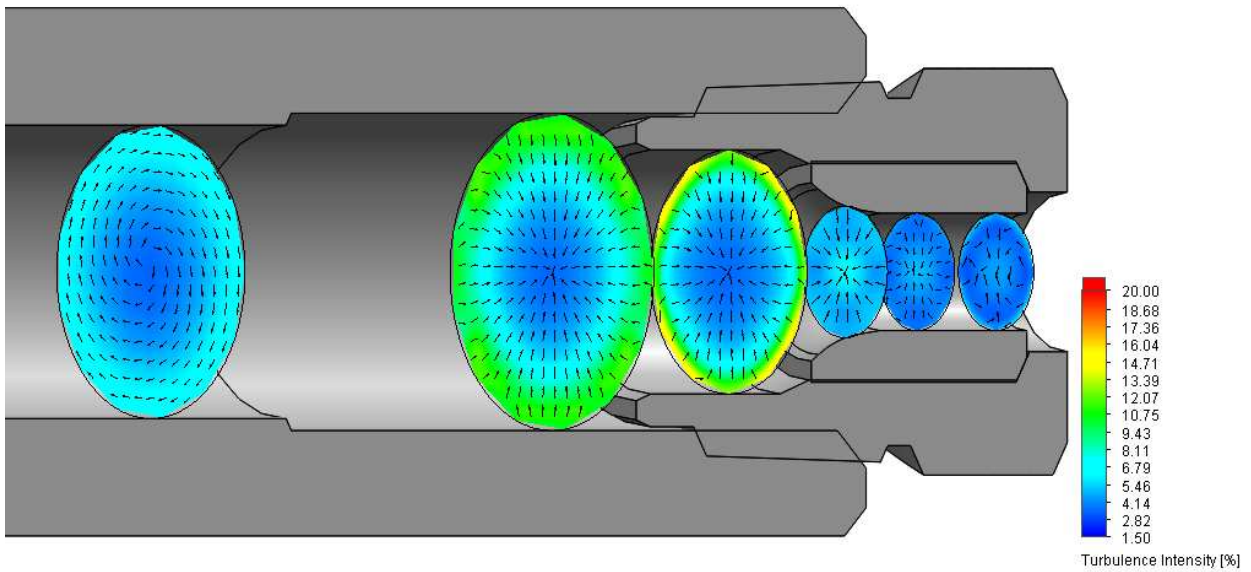


Figure 23: Turbulence Intensity with an Overlay of Velocity Streamlines - Showing 7.9mm (.312") Inside Diameter, 914mm (36") Long Tube with 3.2mm (.125") Orifice